

3.3.2 Number of research papers per teachers in the Journals notified on UGC website during the year

Sarfراز Shaikh

A Novel Ultrasound-Assisted Approach for the Synthesis of Biscoumarin and Bislawsonone Derivatives Using rGO/TiO₂ Nanocomposite as a Heterogeneous Catalyst

Chemistry Africa
https://doi.org/10.1007/s42250-023-00587-6

ORIGINAL ARTICLE



A Novel Ultrasound-Assisted Approach for the Synthesis of Biscoumarin and Bislawsonone Derivatives Using rGO/TiO₂ Nanocomposite as a Heterogeneous Catalyst

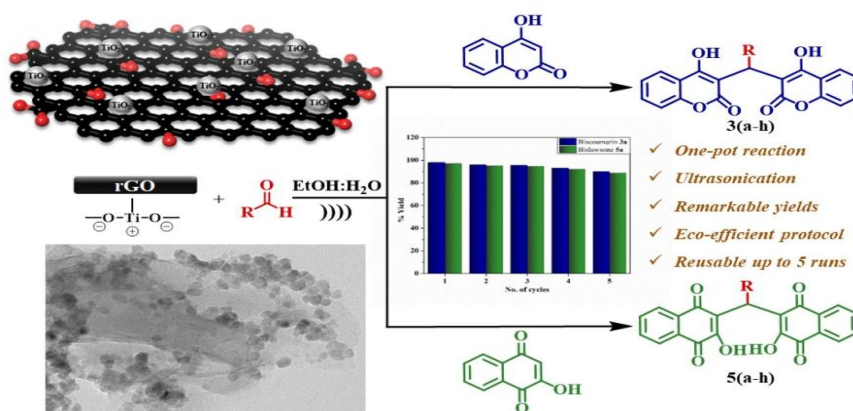
Sarfراز Shaikh^{1,2} · Ishita Yellapurkar¹ · Sonal Bhabal¹ · M. M. V. Ramana¹ · Julekha A. Shaikh³

Received: 7 November 2022 / Accepted: 3 January 2023
© The Tunisian Chemical Society and Springer Nature Switzerland AG 2023

Abstract

In the present study, an efficient and eco-friendly protocol for the syntheses of biscoumarin and bislawsonone derivatives is reported. The reactions are carried out in the presence of the rGO/TiO₂ nanocomposite in an ethanol/water solvent system under the influence of ultrasonication. The structural features of the synthesized reduced graphene oxide (rGO) powder and the catalyst were investigated using FTIR, XRD and Raman characterization techniques, and the morphological analysis is achieved by SEM, TEM imaging and EDX spectroscopy. A detailed examination of the effects of various reaction parameters on the product yield was conducted to develop an optimized procedure for synthesizing several biscoumarin and bislawsonone derivatives. The products were characterized by FTIR, ¹H NMR, Mass spectrometry, and elemental analysis. The significance of this novel protocol is augmented by its notable attributes, namely, shorter reaction times, exceptional product yields, ambient reaction conditions, use of ultrasonication to expedite the reaction, and reusability of the catalyst for up to five cycles. Thus, the environment-friendly nature of the current method abides by the postulates of Green Chemistry.

Graphical Abstract



Keywords Catalysis · rGO/TiO₂ · Biscoumarin · Bislawsonone · Ultrasonication

Extended author information available on the last page of the article

Published online: 10 January 2023

Springer

1 Introduction

Multicomponent reactions (MCRs) are essentially one-pot processes involving three or more components undergoing sequential reactions to yield a single product [1]. Operational simplicity, molecular diversity, atom economy, and convergence of simple starting materials into complex structures grant MCRs a significant status in the world of synthetic organic chemistry [2]. In adherence to the principles of Green Chemistry, numerous catalytic methodologies have been developed for carrying out organic transformations via the MCR route [3]. A plethora of novel methods have been developed for most MCRs that employ heterogeneous catalysts, considering their inherent advantages over homogeneous systems [4, 5]. The use of nanoparticles as catalyst has recently received notable recognition owing to their unique attributes, such as their ability to withstand high temperatures, high recyclability, fine-tuning of the nanomaterial, and the environmentally friendly nature of the catalytic protocol. Thus, nanocatalysis is considered an alternative approach to conventional organic synthesis. The amalgamation of nanocatalysts and MCRs is an advanced strategy for obtaining targeted products with high selectivity within a short period of time [6].

The efficient use of metal oxide nanoparticles as heterogeneous catalysts in MCR has been extensively reported in the literature [7]. To further enhance the sustainability of the experimental protocol, immobilization of the nanocatalyst on a solid support, such as reduced graphene oxide (rGO), has proven to be beneficial [8, 9]. In particular, the rGO/TiO₂ nanocomposite has drawn increasing attention due to its promising features, such as chemical inertness in both acidic and basic media, structural flexibility, and large surface area [10–12]. Comprehensive research has been carried out evaluating the photocatalytic characteristic of rGO/TiO₂ nanocomposite, including dye degradation [13] [14], degradation of VOCs [15] and organic pollutants [16], bisphenol A removal [17], pesticide degradation [18], light-induced selective oxidation [19], etc. However, the use of the nanocomposite to catalyze an MCR has not yet been reported.

Biscoumarins constitute an important class of oxygen-containing heterocycles and are well known for their versatile biological applications, including antibacterial [20], antiviral [21], antimicrobial [22], antioxidant [23], anticancer [24], anticoagulant [25] and enzyme inhibition [23]. Lawsone, 2-hydroxy-1,4-naphthoquinone or hennotannic acid, is the principal dye found in henna leaves (*Lawsonia inermis*) [26]. Traditionally, it has been used in cosmetics as hair dye, tattoo dye, and body paint. Bislawsonone derivatives are bridge-substituted dimers (usually with a phenyl moiety) of lawsone and have significant

pharmacological applications. They are known to exhibit a wide variety of biological activities, including antifungal, antioxidant [27], antileishmanial [28], antibacterial [29], and inhibitory effects on H5N1 neuraminidase [30] and HIV-1 integrase [31]. There are a number of synthetic protocols reported for biscoumarin derivatives using TBAB [32], sodium dodecyl sulfate [33], RuCl₃ [34], heteropolyacids [35], ionic liquid [36] and bislawsonone derivatives using DMAP [37], camphor sulfonic acid [38], humic acid [39], lipase [40], LiCl [41], LiCl coupled with ultrasound or microwave irradiation [42], amino acids [29], sulfamic acid [43] and chitosan [44]. However, these methods suffer from several disadvantages, such as long reaction times, difficult product isolation, no reusability, and inadequate product yields. This necessitates the development of a high-yielding, environmentally benign protocol for the synthesis of biscoumarin and bislawsonone.

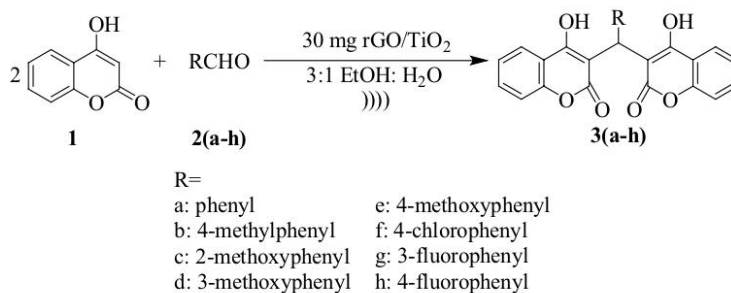
A practical alternative to conventional synthetic methods is using high-energy sources, such as ultrasonication, to accelerate chemical reactions [45]. This high energy causes instantaneous generation and collapse of cavitation bubbles, thereby increasing the temperature and pressure of the reaction medium [46]. Thus, coupling ultrasonication with a nanocatalyst provides an eco-friendly pathway for organic synthesis. Herein, we report the ultrasound-assisted one-pot synthesis of biscoumarin and bislawsonone derivatives catalyzed by rGO/TiO₂ nanocomposite. The catalyst was successfully characterized by FTIR, XRD, Raman, SEM, TEM and EDX techniques. Further, the biscoumarin and bislawsonone derivatives were synthesized and characterized by FTIR, ¹H-NMR, Mass spectrometry and elemental analysis.

2 Experimental

2.1 Materials and methods

Graphite powder, TiO₂ nanopowder and all other chemicals were procured from Sigma Aldrich (India) and used directly without purification. FTIR spectroscopy was performed on Perkin Elmer, Frontier equipment with ATR. X-ray Diffraction studies were carried out on a Shimadzu Maxima 7000 S diffractometer (USA), using Cu K_α radiation in the 2θ range of 10° to 80° at a scanning speed of 5° min⁻¹. The Cu K_α X-ray tube of λ = 1.5418 Å and 1.6 kW power was subjected to 40 kV voltage and 40 mA current. Raman spectra were recorded using Kaiser Optical Systems Inc. (KOSI) laser Raman Spectrometer. SEM analysis and EDX spectroscopy were conducted on JEOL-JSM 7600 field emission gun-scanning electron microscopes operated in the voltage range of 0.1–30 kV. TEM images were recorded on PHILIPS-CM200 electron microscope with an operating voltage of 20–200 kV and a resolution of 2.4 Å. ICP-AES studies were

Scheme 1 Synthesis of biscoumarin derivatives **3(a-h)** using rGO/TiO₂ catalyst (30 mg) in 3:1 EtOH: H₂O (4 mL) under ultrasonication



performed on a HJY Ultima-2 spectrometer (1000 W, 1.29 nebulizer flow, 2.96 nebulizer pressure, 242.795 nm wavelength). The probe sonicator used for ultrasonication was a multi-wave ultrasonic cell crusher (SJA-250 W), equipped with a converter/transducer and a titanium oscillator of 6 mm diameter, and operated at 220 V voltage with a power of 250 W. Melting points were estimated using open capillary tubes and they are uncorrected. For recording of ¹H NMR spectra, Bruker Avance II spectrometer was used. AB SCIEX 3200 QTRAP spectrometer was used for recording of mass spectra in ESI mode. Elemental Analysis (CHN) was accomplished using EA 300 elemental analyser (Euro Vector, Italy).

2.2 Preparation of rGO

Synthesis of rGO was carried out by oxidation of graphite powder according to the modified Hummer's method [47], followed by its reduction to yield reduced graphene oxide (rGO) [48]. About 75 mL of conc. H₂SO₄ was gradually added to a mixture of the commercially acquired graphite powder (1.5 g) and NaNO₃ (1.5 g). After 30 min of stirring, the reaction mixture was cooled by placing it in an ice bath, followed by slow addition of KMnO₄ (9 g) for an hour. This caused a progressive change in the colour of the reaction mixture from black to greenish-black. The ice bath was then removed, and the mixture was stirred for two days to yield brown slurry. To this, warm distilled water (500 mL) was added, followed by slow addition of H₂O₂ (30 mL) to obtain a yellow-coloured suspension. After washing this suspension three times with 6% H₂SO₄ and 1% H₂O₂, several distilled water washings were performed until the pH was neutral. The dark-brown suspension of graphene oxide was exfoliated by mild sonication and centrifugation. During the reduction, the typical weight ratio of hydrazine to graphene oxide was approximately 7:10. The graphene oxide suspension (5 mL) was then stirred in a water bath at 95 °C for an hour with hydrazine (5 μL, 35 wt% in water) and ammonia

solution (35 μL, 28 wt% in water) to obtain black-coloured rGO powder.

2.3 Preparation of rGO/TiO₂ Nanocomposite

A modified version of Men's method [49], as reported by Li et al. [50], was followed without any modifications to prepare the rGO/TiO₂ nanocomposite. The synthesized rGO powder (20 mg) and commercially obtained TiO₂ nanopowder (120 mg) were dispersed in 50 mL of a 4:1 water-ethanol solvent system, sonicated for half an hour and then subjected to hydrothermal treatment at 120 °C for 24 h. The obtained powder was dried under vacuum at 60 °C for 24 h to obtain the rGO/TiO₂ nanocomposite.

2.4 General Procedure for the Synthesis of Biscoumarin Derivatives 3(a-h)

4-hydroxycoumarin **1** (2 mmol) and aromatic aldehyde **2(a-h)** (1 mmol) were added to 3:1 ethanol:water (4 mL) in a round-bottom flask. To this, the rGO/TiO₂ nanocomposite was added (30 mg) and then subjected to ultrasonication (100 W power, 10s/5s on/off time) until completion of the reaction (monitored by TLC). The obtained precipitate was filtered and added to hot ethanol (3 mL) to dissolve the product. The catalyst was then recovered by filtration and the solvent was evaporated off under vacuum to furnish the crude product, which was purified by recrystallization from ethanol (Scheme 1).

3,3'-(phenylmethylene)bis(4-hydroxy-2 H-chromen-2-one) (3a)

Yield 98% (white solid); **MP** = 230–232 °C, **IR** ($\nu_{\text{max}}/\text{cm}^{-1}$): 2980 (OH), 1668, 1652 (C=O). **¹H NMR** (300 MHz, DMSO) δ = 7.90 (s, 1 H, Ar-H), 7.59 (d, J = 5.3 Hz, 2 H, Ar-H), 7.39–7.26 (m, 5 H, Ar-H), 7.20 (d, J = 5.6 Hz, 3 H, Ar-H), 7.15 (s, 2 H, Ar-H), 6.35 (s, 1 H, CH). **MS** (ESI-ve) m/z : 412 (M-H)⁻. **Elemental analysis** for C₂₅H₁₆O₆: C, 72.81; H, 3.91; found: C, 72.76; H, 3.84.

3,3'-(p-tolylmethylene)bis(4-hydroxy-2 H-chromen-2-one) (3b).

Yield 96% (white solid); *MP* = 266–268 °C, **IR** ($\nu_{\max}/\text{cm}^{-1}$): 2913 (OH), 1660, 1652 (C=O). **¹H NMR (300 MHz, DMSO)** δ = 7.89 (d, *J* = 6.5 Hz, 2 H, Ar-H), 7.58 (s, 2 H, Ar-H), 7.35 (d, *J* = 8.4 Hz, 4 H, Ar-H), 7.02 (s, 4 H, Ar-H), 6.30 (s, 1 H, CH), 2.24 (s, 3 H, CH₃). **MS (ESI-ve) m/z**: 426 (M-H)⁻. **Elemental analysis for C₂₆H₁₈O₆**: C, 73.23; H, 4.25; found: C, 73.14; H, 4.17.

3,3'-(2-methoxyphenyl)methylene bis(4-hydroxy-2 H-chromen-2-one) (3c).

Yield 94% (white solid); *MP* = 236 °C, **IR** ($\nu_{\max}/\text{cm}^{-1}$): 2964 (OH), 1644, 1602 (C=O). **¹H NMR (300 MHz, DMSO)** δ = 7.91 (d, *J* = 6.3 Hz, 2 H, Ar-H), 7.58 (s, 2 H, Ar-H), 7.38–7.30 (m, 4 H, Ar-H), 7.16 (s, 2 H, Ar-H), 6.87 (dd, *J* = 12.0, 8.0 Hz, 2 H, Ar-H), 6.25 (s, 1 H, CH), 3.57 (s, 3 H, OCH₃). **MS (ESI-ve) m/z**: 442 (M-H)⁻. **Elemental analysis for C₂₆H₁₈O₇**: C, 70.59; H, 4.10; found: C, 70.41; H, 4.02.

3,3'-(3-methoxyphenyl)methylene bis(4-hydroxy-2 H-chromen-2-one) (3d).

Yield 93% (white solid); *MP* = 238 °C, **IR** ($\nu_{\max}/\text{cm}^{-1}$): 2980 (OH), 1659, 1651 (C=O). **¹H NMR (300 MHz, DMSO)** δ = 7.86 (d, *J* = 6.1 Hz, 2 H, Ar-H), 7.60–7.49 (m, 2 H, Ar-H), 7.37–7.22 (m, 4 H, Ar-H), 7.13 (d, *J* = 9.3 Hz, 1 H, Ar-H), 6.70 (d, *J* = 5.3 Hz, 2 H, Ar-H), 6.63 (s, 1 H, Ar-H), 6.28 (s, 1 H, CH), 3.62 (s, 3 H, OCH₃). **MS (ESI-ve) m/z**: 442 (M-H)⁻. **Elemental analysis for C₂₆H₁₈O₇**: C, 70.59; H, 4.10; found: C, 70.56; H, 3.95.

3,3'-(4-methoxyphenyl)methylene bis(4-hydroxy-2 H-chromen-2-one) (3e).

Yield 96% (white solid); *MP* = 242 °C, **IR** ($\nu_{\max}/\text{cm}^{-1}$): 2981 (OH), 1666, 1660 (C=O). **¹H NMR (300 MHz, DMSO)** δ = 7.88 (s, 2 H, Ar-H), 7.58 (s, 2 H, Ar-H), 7.33 (d, *J* = 5.7 Hz, 4 H, Ar-H), 7.03 (s, 2 H, Ar-H), 6.78 (d, *J* = 4.3 Hz, 2 H, Ar-H), 6.27 (s, 1 H, CH), 3.69 (s, 3 H, OCH₃). **MS (ESI-ve) m/z**: 442 (M-H). **Elemental analysis for C₂₆H₁₈O₇**: C, 70.59; H, 4.10; found: C, 70.54; H, 3.98.

3,3'-(4-chlorophenyl)methylene bis(4-hydroxy-2 H-chromen-2-one) (3f).

Yield 97% (white solid); *MP* = 256–258 °C, **IR** ($\nu_{\max}/\text{cm}^{-1}$): 2980 (OH), 1661, 1603 (C=O). **¹H NMR (300 MHz, DMSO)** δ = 7.89 (s, 2 H, Ar-H), 7.58 (s, 2 H, Ar-H), 7.33 (s, 3 H, Ar-H), 7.26 (d, *J* = 6.9 Hz, 3 H, Ar-H), 7.17 (s, 2 H, Ar-H), 6.31 (s, 1 H, CH). **MS (ESI-ve) m/z**: 446 (M)⁺. **Elemental analysis for C₂₅H₁₅ClO₆**: C, 67.20; H, 3.38; found: C, 67.08; H, 3.25.

3,3'-(3-fluorophenyl)methylene bis(4-hydroxy-2 H-chromen-2-one) (3g).

Yield 97% (white solid); *MP* = 283 °C, **IR** ($\nu_{\max}/\text{cm}^{-1}$): 3065 (OH), 1667, 1606 (C=O). **¹H NMR (300 MHz, DMSO)** δ = 7.88 (d, *J* = 6.8 Hz, 2 H, Ar-H), 7.57 (s, 2 H, Ar-H), 7.34 (d, *J* = 8.0 Hz, 5 H, Ar-H), 6.93 (d, *J* = 20.0 Hz,

3 H, Ar-H), 6.33 (s, 1 H, CH). **MS (ESI-ve) m/z**: 430 (M-H)⁻. **Elemental analysis for C₂₅H₁₅FO₆**: C, 69.77; H, 3.51; found: C, 69.67; H, 3.42.

3,3'-(4-fluorophenyl)methylene bis(4-hydroxy-2 H-chromen-2-one) (3h).

Yield 95% (white solid); *MP* = 213–215 °C, **IR** ($\nu_{\max}/\text{cm}^{-1}$): 2980 (OH), 1667, 1604 (C=O). **¹H NMR (300 MHz, DMSO)** δ = 7.89 (d, *J* = 6.2 Hz, 2 H, Ar-H), 7.58 (s, 2 H, Ar-H), 7.35 (d, *J* = 6.0 Hz, 4 H, Ar-H), 7.16 (s, 2 H, Ar-H), 7.03 (s, 2 H, Ar-H), 6.31 (s, 1 H, CH). **MS (ESI-ve) m/z**: 430 (M-H)⁻. **Elemental analysis for C₂₅H₁₅FO₆**: C, 69.77; H, 3.51; found: C, 69.62; H, 3.40.

2.5 General Procedure for the Synthesis of Bislawsone Derivatives 5(a-h)

2-hydroxy-4-naphthoquinone **4** (2 mmol) and aromatic aldehyde **2(a-h)** (1 mmol) were placed in a round-bottom flask containing 3:1 ethanol:water (4 mL). The rGO/TiO₂ catalyst (30 mg) was then added, and the reaction mixture was subjected to ultrasonication (100 W power, 10s/5s on/off time). Upon completion of the reaction, as indicated by TLC, the reaction mixture was filtered, and the product obtained from the solid residue was dissolved in hot ethanol (3 mL). The catalyst was then filtered, and the crude mass obtained by vacuum evaporation of the solvent was recrystallized with ethanol to yield the purified product (Scheme 2).

3,3'-(phenylmethylene)bis(2-hydroxynaphthalene-1,4-dione) (5a).

Yield 97% (Yellow solid); *MP* = 202–204 °C, **IR** ($\nu_{\max}/\text{cm}^{-1}$): 3327 (OH), 1658, 1643 (C=O). **¹H NMR (300 MHz, CDCl₃)** δ = 8.11 (d, *J* = 4.7 Hz, 7 H, Ar-H), 7.74 (dd, *J* = 11.5, 3.9 Hz, 6 H, Ar-H), 6.27 (s, 1 H, CH). **MS (ESI-ve) m/z**: 436 (M-H)⁻. **Elemental analysis for C₂₇H₁₆O₆**: C, 74.31; H, 3.70; found: C, 74.25; H, 3.62.

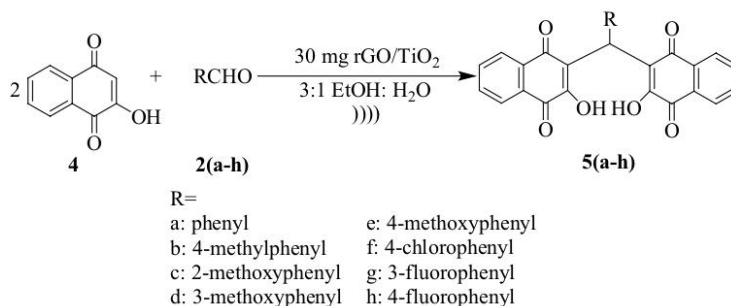
3,3'-(p-tolylmethylene)bis(2-hydroxynaphthalene-1,4-dione) (5b).

Yield 94% (Yellow solid); *MP* = 174–176 °C, **IR** ($\nu_{\max}/\text{cm}^{-1}$): 3355 (OH), 1620, 1608 (C=O). **¹H NMR (300 MHz, DMSO)** δ = 7.99–7.90 (m, 4 H, Ar-H), 7.78 (s, 4 H, Ar-H), 7.03 (d, *J* = 27.6 Hz, 4 H, Ar-H), 5.97 (s, 1 H, CH), 2.23 (s, 3 H, CH₃). **MS (ESI + ve) m/z**: 450 (M + H)⁺. **Elemental analysis for C₂₈H₁₈O₆**: C, 74.66; H, 4.03; found: C, 74.51; H, 3.94.

3,3'-(2-methoxyphenyl)methylene bis(2-hydroxynaphthalene-1,4-dione) (5c).

Yield 95% (Yellow solid); *MP* = 212–214 °C, **IR** ($\nu_{\max}/\text{cm}^{-1}$): 3293 (OH), 1659, 1634 (C=O). **¹H NMR (300 MHz, DMSO)** δ = 7.93 (d, *J* = 19.2 Hz, 4 H, Ar-H), 7.79 (s, 4 H, Ar-H), 7.09 (d, *J* = 20.9 Hz, 2 H, Ar-H), 6.82 (d, *J* = 31.1 Hz, 2 H, Ar-H), 6.04 (s, 1 H, CH), 3.65 (s, 3 H, OCH₃). **MS (ESI) m/z**: 466 (M)⁺. **Elemental analysis for C₂₈H₁₈O₇**: C, 72.10; H, 3.89; found: C, 72.03; H, 3.72.

Scheme 2 Synthesis of bislawnone derivatives **5(a-h)** using rGO/TiO₂ catalyst (30 mg) in 3:1 EtOH: H₂O (4 mL) under ultrasonication



3,3'-((3-methoxyphenyl)methylene)bis(2-hydroxynaphthalene-1,4-dione) (5d).

Yield 94% (Yellow solid); *MP* = 190–192 °C, IR ($\nu_{\max}/\text{cm}^{-1}$): 3061 (OH), 1613, 1593 (C=O). ¹H NMR (300 MHz, CDCl₃) δ = 8.10 (s, 4 H, Ar-H), 7.79–7.66 (m, 4 H, Ar-H), 7.23 (s, 1 H, Ar-H), 6.82 (dd, *J* = 18.3, 10.6 Hz, 3 H, Ar-H), 6.24 (s, 1 H, CH), 3.76 (s, 3 H, OCH₃). MS (ESI-ve) *m/z*: 466 (M-H)⁻. Elemental analysis for C₂₈H₁₈O₇: C, 72.10; H, 3.89; found: C, 72.01; H, 3.69.

3,3'-((4-methoxyphenyl)methylene)bis(2-hydroxynaphthalene-1,4-dione) (5e).

Yield 93% (Yellow solid); *MP* = 220–222 °C, IR ($\nu_{\max}/\text{cm}^{-1}$): 3394 (OH), 1665, 1634 (C=O). ¹H NMR (300 MHz, CDCl₃) δ = 8.11 (d, *J* = 6.6 Hz, 4 H, Ar-H), 7.72 (dd, *J* = 15.3, 7.7 Hz, 4 H, Ar-H), 7.22 (d, *J* = 8.1 Hz, 2 H, Ar-H), 6.84 (d, *J* = 6.4 Hz, 2 H, Ar-H), 6.18 (s, 1 H, CH), 3.79 (s, 3 H, OCH₃). MS (ESI-ve) *m/z*: 466 (M-H)⁻. Elemental analysis for C₂₈H₁₈O₇: C, 72.10; H, 3.89; found: C, 72.04; H, 3.74.

3,3'-((4-chlorophenyl)methylene)bis(2-hydroxynaphthalene-1,4-dione) (5f).

Yield 96% (Yellow solid); *MP* = 188–190 °C, IR ($\nu_{\max}/\text{cm}^{-1}$): 3155 (OH), 1639, 1631 (C=O). ¹H NMR (300 MHz, CDCl₃) δ = 8.09 (s, 5 H, Ar-H), 7.75 (s, 2 H, Ar-H), 7.24 (s, 5 H, Ar-H), 6.17 (s, 1 H, CH). MS (ESI + ve) *m/z*: 470 (M+H)⁺. Elemental analysis for C₂₇H₁₅ClO₆: C, 68.87; H, 3.21; O, 20.39; found: C, 68.75; H, 3.14; O, 20.24.

3,3'-((3-fluorophenyl)methylene)bis(2-hydroxynaphthalene-1,4-dione) (5g).

Yield 97% (Yellow solid); *MP* = 213–215 °C, IR ($\nu_{\max}/\text{cm}^{-1}$): 3422 (OH), 1654, 1640 (C=O). ¹H NMR (300 MHz, CDCl₃) δ = 8.11 (s, 4 H, Ar-H), 7.79–7.68 (m, 4 H, Ar-H), 7.25 (s, 1 H, Ar-H), 7.08 (d, *J* = 4.9 Hz, 1 H, Ar-H), 7.02–6.90 (m, 2 H, Ar-H), 6.23 (s, 1 H, CH). MS (ESI + ve) *m/z*: 454 (M+H)⁺. Elemental analysis for C₂₇H₁₅FO₆: C, 68.82; H, 3.19; found: C, 68.75; H, 3.11.

3,3'-((4-fluorophenyl)methylene)bis(2-hydroxynaphthalene-1,4-dione) (5h).

Yield 96% (Yellow solid); *MP* = 193–195 °C, IR ($\nu_{\max}/\text{cm}^{-1}$): 3333 (OH), 1669, 1640 (C=O). ¹H NMR (300 MHz, CDCl₃) δ = 8.10 (s, 5 H, Ar-H), 7.81–7.62 (m, 5 H, Ar-H), 6.98 (s, 2 H, Ar-H), 6.18 (s, 1 H, CH). MS (ESI + ve) *m/z*: 454 (M+H)⁺. Elemental analysis for C₂₇H₁₅FO₆: C, 71.37; H, 3.33; found: C, 71.21; H, 3.28.

3 Results and Discussion

3.1 Characterization of rGO and rGO/TiO₂ Nanocomposite

3.1.1 Fourier Transform Infrared Spectroscopy (FTIR)

FTIR spectroscopic analysis of rGO (Fig. 1a) and the rGO/TiO₂ nanocomposite (Fig. 1b) was performed for the detection of functional groups and characterization of the

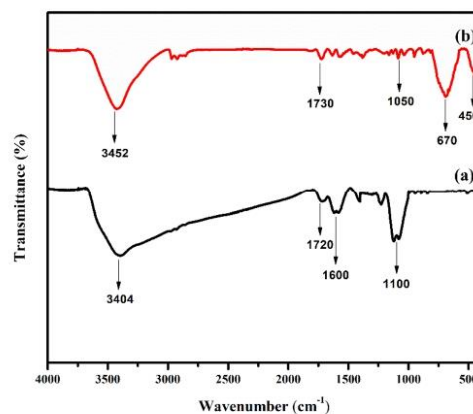


Fig. 1 FTIR spectra of **a** rGO and **b** rGO/TiO₂ nanocomposite using a powder sample

covalent bonding information [51]. The broad peaks at around 3400 cm^{-1} are attributed to the stretching vibrations of the surface hydroxyl groups. The peaks at around 1700 cm^{-1} correspond to the carbonyl functional group, whereas the peaks at 1100 cm^{-1} in Fig. 1a and 1050 cm^{-1} in Fig. 1b are accredited to C–O stretching vibrations. In Fig. 1a, the peak observed at around 1600 cm^{-1} corresponds to the skeletal vibrations of the rGO sheet [52]. The presence of oxygen-containing functional groups in Fig. 1b suggests partial reduction of graphene, thereby facilitating the interaction of TiO_2 with these groups [53]. The characteristic peaks of Ti–O–Ti vibrations are observed at 670 cm^{-1} and 450 cm^{-1} in the spectrum of the nanocomposite (Fig. 1b).

3.1.2 X-Ray Diffraction (XRD)

X-Ray Diffraction Studies of rGO (Fig. 2a) and rGO/ TiO_2 nanocomposite (Fig. 2b) were carried out to determine the crystallographic structure. The peaks at $2\theta = 24.4^\circ$ and 44° corresponding to the (002) and (100) planes, respectively, observed in Fig. 2a, are characteristic of a typical graphitic structure [54]. The diffraction pattern of the nanocomposite (Fig. 2b) suggests the formation of anatase TiO_2 nanoparticles (JCPDS 21-1272). The peaks at $2\theta = 25.3^\circ$, 37.9° , 48° , 54.3° , and 62.9° can be indexed to the (101), (004), (200), (105), and (204) reflection planes, respectively. The low intensity of these peaks is accredited to the use of ultrasonication during the synthesis of the nanocomposite [55]. Moreover, shielding of the (002) peak of rGO at 24.4° by the (101) peak of TiO_2 at 25.3° in the nanocomposite is a commonly observed phenomenon [56].

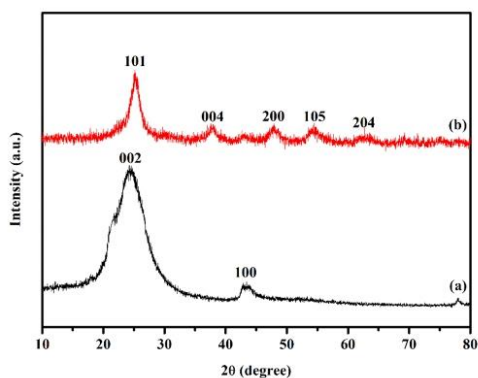


Fig. 2 X-ray diffraction pattern of **a** rGO and **b** rGO/ TiO_2 nanocomposite using a powder sample from 10° to 80° 2θ range at scanning speed of 5 min^{-1}

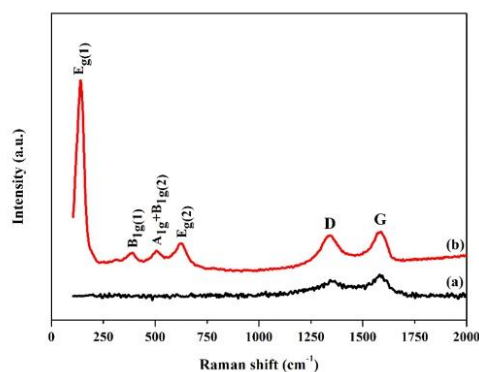


Fig. 3 Raman spectra of **a** rGO and **b** rGO/ TiO_2 nanocomposite using a powder sample

3.1.3 Raman Spectroscopy

Raman Spectroscopy is one of the most powerful non-destructive tools used to characterize graphitic materials. Figure 3b shows the phonon bands of anatase TiO_2 at 144 cm^{-1} , 396 cm^{-1} , 512 cm^{-1} and 631 cm^{-1} , corresponding to the $E_{g(1)}$, B_{1g} , $A_{1g} + B_{1g}$, and $E_{g(2)}$ transitions, respectively [57]. Furthermore, the spectra exhibit two characteristic bands: the D-band (sp^3 defects) and the G-band (in-plane vibrations of sp^2 atoms) [58]. In rGO (Fig. 3a), these bands were obtained at 1341 cm^{-1} and 1580 cm^{-1} , while in the nanocomposite (Fig. 3b), they were at 1353 cm^{-1} and 1589 cm^{-1} , respectively. The red shift observed in these bands can be attributed to the presence of hydroxyl groups on the surface of the nanocomposite. Correspondingly, the I_D/I_G ratio increased from 0.77 in rGO to 0.94 in rGO/ TiO_2 as structural defects in two-dimensional graphitic sheets increased with the incorporation of TiO_2 [59, 60].

3.1.4 Morphology

The morphological features of rGO and rGO/ TiO_2 nanocomposite were investigated using SEM, TEM and EDX characterization techniques. The SEM image of rGO (Fig. 4a) shows a two-dimensional layered structure of graphene sheets with curved edges, while that of the nanocomposite (Fig. 4b) depicts the rGO sheets as well-decorated and embedded with TiO_2 nanoparticles. Further, TEM analysis was carried out for detailed structural examination. Figure 5a portrays the smooth and somewhat wrinkled graphene layers of rGO, and Fig. 5b illustrates the TiO_2 nanoparticles anchored and aggregated over the rGO sheets. EDX spectroscopy (Fig. 6) revealed

Fig. 4 SEM images of **a** rGO and **b** rGO/TiO₂ nanocomposite using a small portion of the powder dispersed in ethanol, transferred to the adhesive carbon tape, and air-drying

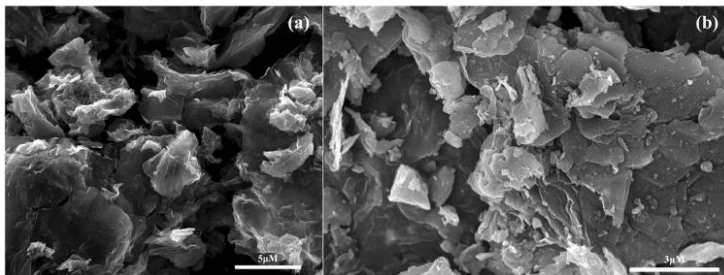


Fig. 5 TEM images of **a** rGO and **b** rGO/TiO₂ nanocomposite by dispersing a small portion in ethanol and transferring it to the copper grid and air-drying

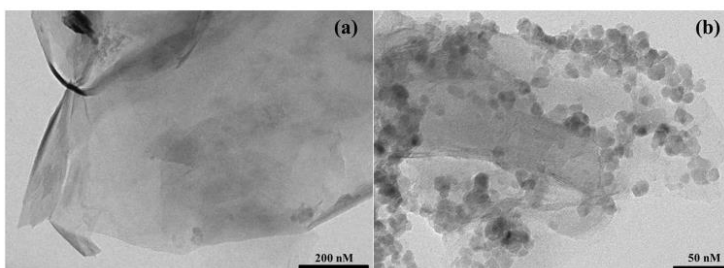
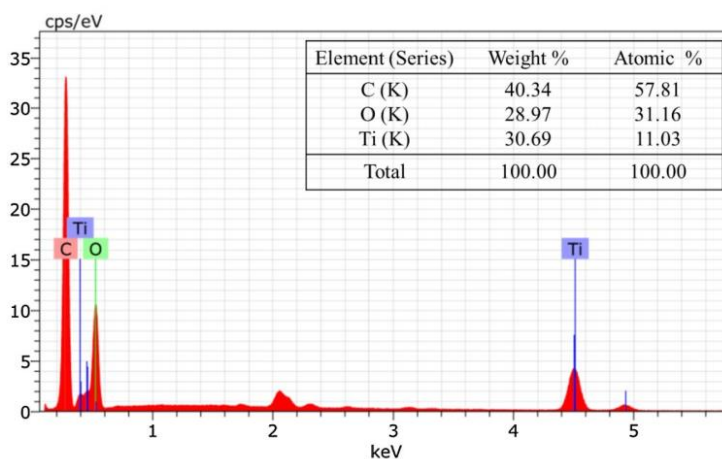


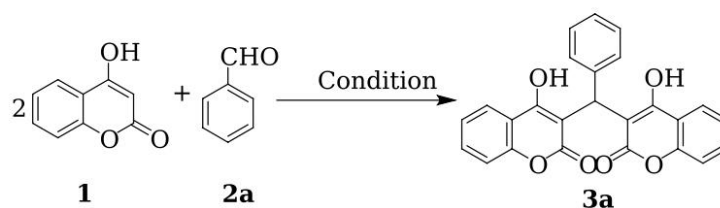
Fig. 6 EDX spectrum of rGO/TiO₂ nanocomposite using a small portion of the powder dispersed in ethanol and transferring to the adhesive carbon tape and air-drying



the elemental composition of the nanocomposite, with 57.81% of C, 31.16% of O and 11.03% of Ti. Other than the detected elements, no other impurities were detected inferring that the synthesized nanocomposite is in high purity.

3.2 Catalytic Performance of rGO/TiO₂ Nanocomposite

To develop an efficient synthetic protocol, various reaction parameters, such as the amount of catalyst, solvent and solvent systems, and temperature were optimized by

Table 1 Optimization of reaction parameters for the synthesis of **3a**

Entry	Catalyst	Solvent	Condition ^a	% yield ^c
1	No catalyst	Ethanol	US probe	20
2	rGO (30 mg)	Ethanol	US probe	26
3	Bulk TiO ₂ (30 mg)	Ethanol	US probe	25
4	Commercial TiO ₂ NPs (30 mg)	Ethanol	US probe	48
5	rGO/TiO ₂ (30 mg)	Ethanol	US probe	77
6	rGO/TiO ₂ (20 mg)	Ethanol	US probe	62
7	rGO/TiO ₂ (40 mg)	Ethanol	US probe	77
8	rGO/TiO ₂ (30 mg)	Methanol	US probe	72
9	rGO/TiO ₂ (30 mg)	Water	US probe	47
10	rGO/TiO ₂ (30 mg)	Acetonitrile	US probe	45
11	rGO/TiO ₂ (30 mg)	Dichloromethane	US probe	40
12	rGO/TiO ₂ (30 mg)	Toluene	US probe	38
13	rGO/TiO₂ (30 mg)	Ethanol:Water (3:1)	US probe	98
14	rGO/TiO ₂ (30 mg)	Ethanol:Water (2:1)	US probe	76
15	rGO/TiO ₂ (30 mg)	Ethanol:Water (1:1)	US probe	70
16	rGO/TiO ₂ (30 mg)	Ethanol:Water (1:2)	US probe	58
17	rGO/TiO ₂ (30 mg)	Ethanol:Water (1:3)	US probe	50
18	rGO/TiO ₂ (30 mg)	Ethanol:Water (3:1)	25 °C ^b	35
19	rGO/TiO ₂ (30 mg)	Ethanol:Water (3:1)	50 °C	55
20	rGO/TiO ₂ (30 mg)	Ethanol:Water (3:1)	75 °C	64
21	rGO/TiO ₂ (30 mg)	Ethanol:Water (3:1)	US bath	56

Bold indicates best optimum condition for the present synthetic strategy

^aAll reactions were carried out for 5 min except for

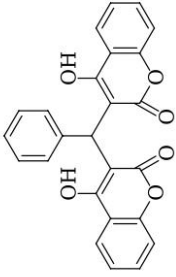
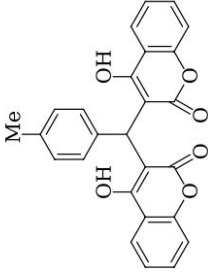
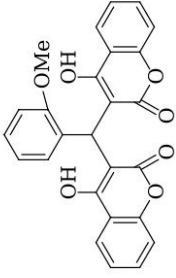
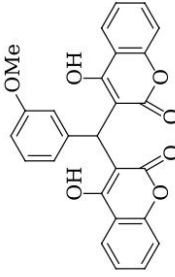
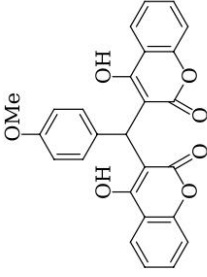
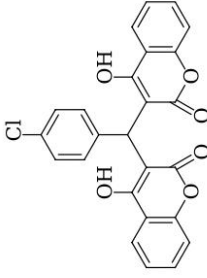
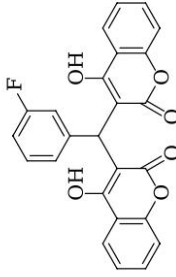
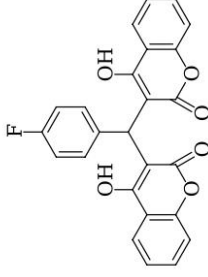
^bEntry 18 which was carried out for 30 min

^cIsolated yield

considering the reaction between 4-hydroxycoumarin and benzaldehyde as a module (Table 1). Foremost, the use of the catalyst was substantiated by carrying out the reaction in its absence. The reaction did not proceed well, and about 20% of the product was obtained (Table 1, entry 1). Moreover, using the synthesized rGO powder as a catalyst resulted in a low yield (Table 1, entry 2). The use of commercially procured bulk and nano TiO₂ also resulted in poor yields (Table 1, entries 3 and 4). The rGO/TiO₂ nanocomposite was then utilized as a heterogeneous catalyst, resulting in a somewhat acceptable product yield of 77% (Table 1, entry 5). The effect of catalyst loading was then investigated by varying the amount of nanocomposite added from 20 mg to

40 mg (Table 1, entries 6 and 7). It was observed that 30 mg of the catalyst was optimal, and increasing or decreasing the amount of catalyst yielded substandard results. Thus, 30 mg of rGO/TiO₂ was used for further investigation. To study the effect of solvents, protic solvents such as ethanol, methanol, and water and aprotic solvents such as acetonitrile, dichloromethane, and toluene were used. The highest yield was observed for ethanol (Table 1, entry 5), followed by methanol and water (Table 1, entries 8 and 9, respectively); aprotic solvents resulted in lower yields (Table 1, entries 10–12). Interestingly, the water-ethanol solvent system granted excellent results (Table 1, entries 13–17). Upon careful examination, it was found that 3:1 ethanol:water afforded

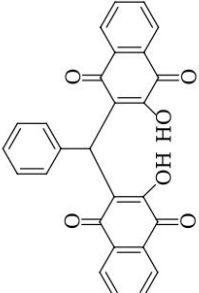
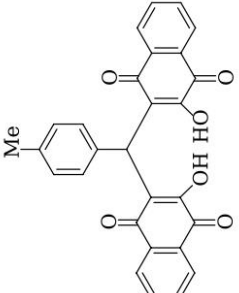
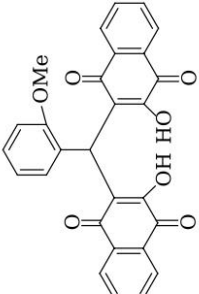
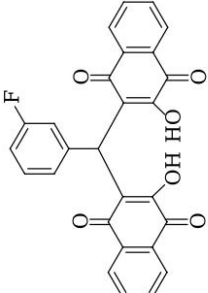
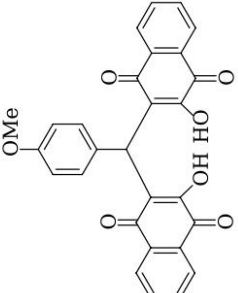
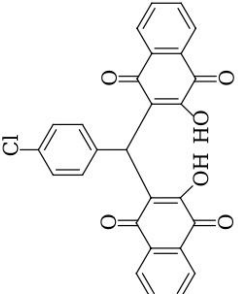
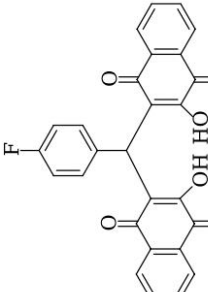
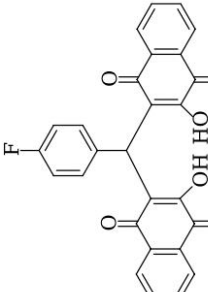
Table 2 Synthesis of biscoumarin derivatives **3(a-h)** using rGO/TiO₂ nanocomposite under optimized reaction conditions

		
3a (5 min, 98%^a)	3b (5 min, 96%^a)	3c (6 min, 94%^a)
		
3d (6 min, 93%^a)	3e (5.5 min, 96%^a)	3f (5 min, 97%^a)
		
3g (7.5 min, 97%^a)	3h (7 min, 95%^a)	

Reaction conditions: 4-hydroxycoumarin (2 mmol), aldehyde (1 mmol) and catalyst (30 mg) under ultrasonication at room temperature

^aIsolated yield

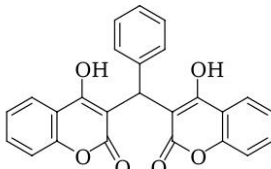
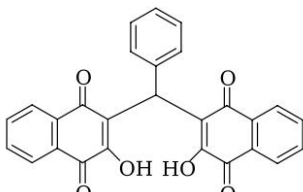
Table 3 Synthesis of bislawsone derivatives **5(a-h)** using rGO/TiO₂ nanocomposite under optimized reaction conditions

 <p>5a (5 min, 97%^a)</p>	 <p>5b (5.5 min, 94%^a)</p>	 <p>5c (6 min, 95%^a)</p>
 <p>5d (5 min, 94%^a)</p>	 <p>5e (6.5 min, 93%^a)</p>	 <p>5f (6 min, 96%^a)</p>
 <p>5g (8 min, 97%^a)</p>	 <p>5h (8 min, 96%^a)</p>	

Reaction conditions: 2-hydroxy-4-naphthoquinone (2 mmol), aldehyde (1 mmol) and catalyst (30 mg) under ultrasonication at room temperature

^aIsolated yield

Table 4 Comparative study of rGO/TiO₂ nanocomposite for the synthesis of biscoumarin and bislawsone derivatives

Entry	Product	Catalyst	Condition	Yield (%)	Refs.
1		TiO ₂ /KSF (20 mg)	Neat, 100 °C, 10 min	98	[61]
2		RuCl ₃ (5 mol%)	Water, 80 °C, 25 min	84	[34]
3		DBSA (25 mol%)	1:1 EtOH:H ₂ O, MW, 12 min	95	[62]
4		[bmim]BF ₄ (4 eq.)	Neat, 60–70 °C, 2 h	84	[36]
5		BiVO ₄ (30 mg)	Water, 80 °C, 25 min	98	[63]
6		TBAB (10 mol%)	Water, reflux, 25 min	92	[32]
7		Nano TiO ₂ (5 mol%)	Water, reflux, 8 min	90	[64]
8		Graphene oxide (5 mg)	Water, reflux, 25 min	90	[65]
9		rGO/TiO₂ (30 mg)	3:1 EtOH:H₂O, US, 5 min	98	This work
10		Lipase (30 mg)	Ethanol, 60 °C, 2 h	88	[40]
11		Et ₃ N (1 eq.)	Ethanol, 25 °C, 5 min	75	[66]
12		Humic acid (10 mg)	Neat, 100 °C, 15 min	96	[39]
13		CSA (20 mol%)	1:1 EtOH:H ₂ O, 27 °C, 2 h	94	[38]
14		LiCl (1 eq.)	Water, 25 °C, 12 h	83	[41]
15		β-alanine (15 mg)	AcOH, Ar atm, reflux, 5 h	83	[28]
16		Sulfamic acid (20 mol%)	1:1 EtOH:H ₂ O, 25 °C, 16 h	92	[43]
17		DMAP (20 mol%)	EtOH, MW, reflux, 15 min	96	[37]
18		rGO/TiO₂ (30 mg)	3:1 EtOH:H₂O, US, 5 min	97	This work

Bold indicates best optimum condition for the present synthetic strategy

an exceptional product yield of 98% (Table 1, entry 13). Furthermore, the reaction was performed under reflux conditions as well as in an ultrasonic bath to authenticate the use of probe ultrasonication. Insufficient yields were observed under thermal conditions (Table 1, entries 18–20), and the ultrasonic bath resulted in a slightly better but inadequate yield (Table 1, entry 21). Thus, to demonstrate its generality, the optimized protocol was employed to synthesize eight biscoumarin derivatives **3(a-h)** by varying the aromatic aldehyde. Table 2 lists the reaction times and the isolated yields of the derivatives. It was observed that the nature of the aldehyde (electron-rich or electron-poor) did not affect

the general outcome of the reaction, and all products were obtained in high yields in a short amount of time.

Encouraged by these phenomenal observations, the scope of this novel methodology was assessed by replacing 4-hydroxycoumarin with 2-hydroxy-1,4-naphthoquinone and synthesizing bislawsone derivatives. A total of eight products **5(a-h)** were obtained with exceptional yields using a diverse array of aldehydes, as delineated in Table 3.

Fig. 7 Plausible mechanism for biscoumarin and bislawsone synthesis in the presence of rGO/TiO₂ nanocomposite

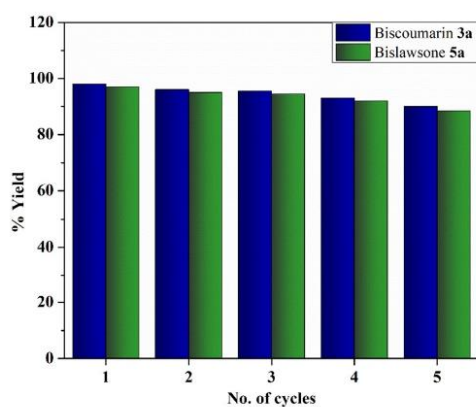
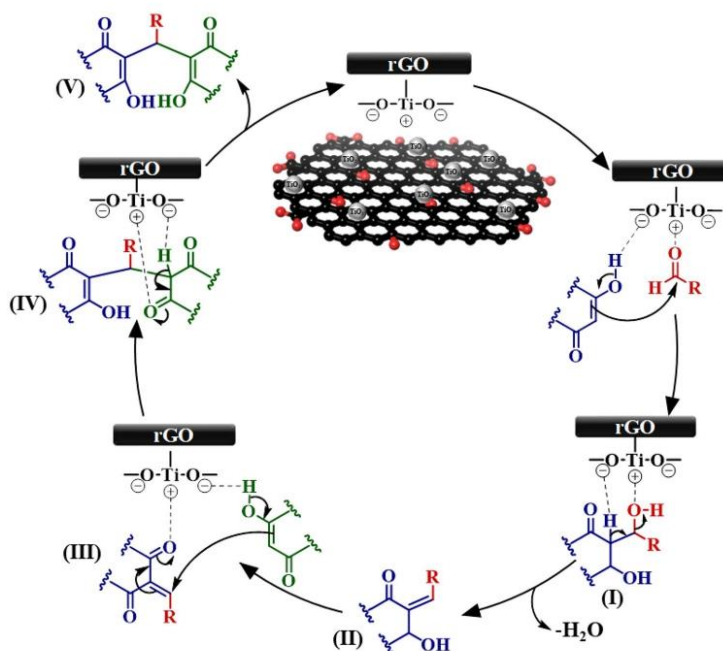


Fig. 8 Recyclability of the rGO/TiO₂ catalyst. Reaction conditions: 4-hydroxycoumarin/2-hydroxy-4-naphthoquinone (2 mmol), benzaldehyde (1 mmol) and catalyst (30 mg) under ultrasonication at room temperature

3.3 Comparative Study

To establish the merits of the rGO/TiO₂ nanocomposite as a heterogeneous catalyst, a study was conducted to compare the efficiency of the current protocol with those previously reported in the literature, as depicted in Table 4. The reaction parameters considered for comparison were the nature and amount of catalyst used, nature of the solvent used, reaction temperature and time, product yields, and utilization of non-conventional alternatives such as ionic liquids, microwave irradiation, or ultrasonication to spike the reaction rate. It is evident that despite the observed versatility, the reported protocols suffer from numerous drawbacks, such as high reaction temperature and time, inadequate product yield, harsh reaction conditions, and the requirement of an inert atmosphere. The present work supersedes all these difficulties and thus validates the efficacy of this novel methodology.

3.4 Plausible Mechanism

Figure 7 outlines a plausible mechanism for rGO/TiO₂ catalyzed biscoumarin and bislawsone synthesis. Initially, the carbonyl group of the aldehyde is activated by Ti⁴⁺, facilitating nucleophilic attack of the carbon atom of 4-hydroxycoumarin/2-hydroxy-4-naphthoquinone on the aldehyde to form intermediate **I**. Subsequently, a water molecule is lost to yield enol **II**, which tautomerizes to its keto form **III**. Ti⁴⁺ then activates intermediate **III**, followed by a nucleophilic attack from another 4-hydroxycoumarin/2-hydroxy-4-naphthoquinone molecule, forming intermediate **IV**. Finally, another keto-enol tautomerization leads to the formation of the desired product **V**, regenerating the catalyst.

3.5 Recyclability Study

The ability to catalyze multiple reaction cycles without significantly affecting the reaction outcome is one of the fundamentals of catalysis. Model reactions of 4-hydroxycoumarin and benzaldehyde for the synthesis of biscoumarin **3a** and 2-hydroxy-4-naphthoquinone and benzaldehyde for the synthesis of bislawsone **5a** were employed to ascertain the reusability of the catalyst. On completing the reaction, as mentioned in Schemes 1 and 2, the catalyst was isolated via filtration, washed several times with hot ethanol, dried in an oven, and then reused. As illustrated in Fig. 8, the efficiency of the rGO/TiO₂ nanocomposite remained unaltered for up to five catalytic runs for both biscoumarin **3a** and bislawsone **5a**. Leaching of TiO₂ nanoparticles into the reaction mixture was also analyzed with ICP-AES analysis. For this purpose, blank rGO/TiO₂ nanocomposite in 3:1 EtOH:H₂O was taken and the sample was ultrasonicated for 5 min. The solvent was analysed using ICP-AES and it was found that Ti concentration in the solution was less than the detection limit. Similar results were obtained when the completed reaction mixture was filtered and the solvent was analysed. Both findings indicate that the TiO₂ nanoparticles did not leach into the solution during the catalytic cycles and thus, remained intact on the rGO support. The eventual decline observed in the efficacy of the catalyst may be accredited to agglomeration of the nanomaterial or minor inadequacies in the recovery process.

4 Conclusion

In conclusion, a novel ultrasound-assisted procedure was developed for the efficient synthesis of biscoumarin and bislawsone derivatives catalyzed by rGO/TiO₂ nanocomposite. The catalyst was characterized by FTIR, XRD, Raman, SEM, TEM and EDX techniques. FTIR, XRD, and Raman analyses were used to verify the structural features. SEM

and TEM imaging were used to determine the morphological attributes, and EDX spectroscopy was used to examine the elemental composition. The reaction parameters were optimized, and several biscoumarin and bislawsone derivatives were synthesized. The sustainable nature of the current synthetic protocol pays heed to the postulates of Green Chemistry i.e. ambient reaction temperature, short reaction time, use of green solvents, extraordinary product yield, and reusability of the catalyst for five cycles and hence, offers an environmentally attractive approach to conventional synthesis.

Supplementary Information The online version contains supplementary material available at <https://doi.org/10.1007/s42250-023-00587-6>.

Acknowledgements We are thankful to Microanalytical Laboratory, University of Mumbai for providing characterization facilities. Authors also acknowledge SAIF (IITB), Mumbai.

Author Contributions SS and YY contributed to the design and implementation of the research, to the analysis of the results and writing of the manuscript. SB and JS contributed to the interpretation of the results to the writing and review of the manuscript.

Funding Not applicable.

Declarations

Conflict of Interest The authors declare that there are no financial or commercial conflicts of interest that could have appeared to influence the work stated in this paper.

Ethical Approval Not applicable.

References

- Dömling A (2005) The discovery of new isocyanide-based multicomponent reactions. In: Zhu J, Bienaymé H (eds) Multicomponent reactions. Wiley, New York, pp 76–94. <https://doi.org/10.1002/3527605118.ch3>
- Abranches PA, da Paiva S, de Fátima WF et al (2018) Calix[*n*] arene-Catalyzed three-component Povarov reaction: microwave-assisted synthesis of Julolidines and mechanistic insights. *J Org Chem* 83(4):1761–1771. <https://doi.org/10.1021/acs.joc.7b02532>
- Neto BAD, Rocha RO, Rodrigues MO (2021) Catalytic approaches to multicomponent reactions: a critical review and perspectives on the roles of catalysis. *Molecules* 27(1):132–159. <https://doi.org/10.3390/molecules27010132>
- Kerru N, Bhaskaruni SVHS, Gummidi L et al (2019) Recent advances in heterogeneous catalysts for the synthesis of imidazole derivatives. *Synth Commun* 49(19):2437–2459. <https://doi.org/10.1080/00397911.2019.1639755>
- Climent MJ, Corma A, Iborra S (2012) Homogeneous and heterogeneous catalysts for multicomponent reactions. *RSC Adv* 2(1):16–58. <https://doi.org/10.1039/C1RA00807B>
- Behraves S, Fareghi-Alamdari R, Badri R (2018) Sulfonated reduced graphene oxide (rGO-SO₃H): as an efficient nanocatalyst for one-pot synthesis of 2-amino-3-cyano-7-hydroxy-4H-chromenes derivatives in water. *Polycycl Aromat Compd* 38(1):51–65. <https://doi.org/10.1080/10406638.2016.1149080>

7. Wang S, Wang Z, Zha Z (2009) Metal nanoparticles or metal oxide nanoparticles, an efficient and promising family of novel heterogeneous catalysts in organic synthesis. *Dalton Trans* 43:9363–9373. <https://doi.org/10.1039/B913539A>
8. Sankar M, He Q, Engel R et al (2020) Role of the support in gold-containing nanoparticles as heterogeneous catalysts. *Chem Rev* 120(8):3890–3938. <https://doi.org/10.1021/acs.chemrev.9b00662>
9. Demirkan B, Bozkurt S, Şavk A et al (2019) Composites of bimetallic platinum-cobalt alloy nanoparticles and reduced graphene oxide for electrochemical determination of ascorbic acid, dopamine, and uric acid. *Sci Rep* 9:12258–12264. <https://doi.org/10.1038/s41598-019-48802-0>
10. Leary R, Westwood A (2011) Carbonaceous nanomaterials for the enhancement of TiO₂ photocatalysis. *Carbon* 49(3):741–772. <https://doi.org/10.1016/j.carbon.2010.10.010>
11. Morales-Torres S, Pastrana-Martínez LM, Figueiredo JL, Faria JL et al (2012) Design of graphene-based TiO₂ photocatalysts—a review. *Environ Sci Pollut Res* 19(9):3676–3687. <https://doi.org/10.1007/s11356-012-0939-4>
12. Balsamo S, Fiorenza R, Condorelli M et al (2021) One-pot synthesis of TiO₂-rGO photocatalysts for the degradation of groundwater pollutants. *Materials* 14(20):5938–5956. <https://doi.org/10.3390/ma14205938>
13. Ali MHH, Al-Afiy AD, Goher ME (2018) Preparation and characterization of graphene – TiO₂ nanocomposite for enhanced photodegradation of Rhodamine-B dye. *Egypt J Aquat Res* 44(4):263–270. <https://doi.org/10.1016/j.ejar.2018.11.009>
14. Kocijan M, Čurković L, Bdiik I et al (2022) Immobilised rGO/TiO₂ nanocomposite for multi-cycle removal of methylene blue dye from an aqueous medium. *Appl Sci* 12(1):385–398. <https://doi.org/10.3390/app12010385>
15. Lin W, Xie X, Wang X et al (2018) Efficient adsorption and sustainable degradation of gaseous acetaldehyde and o-xylene using rGO-TiO₂ photocatalyst. *Chem Eng J* 349:708–718. <https://doi.org/10.1016/j.cej.2018.05.107>
16. Kocijan M, Čurković L, Gonçalves G et al (2022) The potential of rGO@TiO₂ photocatalyst for the degradation of organic pollutants in water. *Sustainability* 14(19):12703–12721. <https://doi.org/10.3390/su141912703>
17. Xu L, Yang L, Johansson EMJ et al (2018) Photocatalytic activity and mechanism of bisphenol A removal over TiO₂/rGO nanocomposite driven by visible light. *Chem Eng J* 350:1043–1055. <https://doi.org/10.1016/j.cej.2018.06.046>
18. Luna-Sanguino G, Ruáz-DeIgado A, Tolosana-Moranchel A et al (2020) Solar photocatalytic degradation of pesticides over TiO₂-rGO nanocomposites at pilot plant scale. *Sci Total Environ* 737:140286–140390. <https://doi.org/10.1016/j.scitotenv.2020.140286>
19. Yuan L, Yu Q, Zhang Y et al (2014) Graphene–TiO₂ nanocomposite photocatalysts for selective organic synthesis in water under simulated solar light irradiation. *RSC Adv* 4(29):15264–15270. <https://doi.org/10.1039/C4RA01190B>
20. Li J, Xue X, Li X et al (2016) Synthesis of biscoumarin and dihydropyran derivatives as two novel classes of potential anti-bacterial derivatives. *Arch Pharm Res* 39(10):1349–1355. <https://doi.org/10.1007/s12272-015-0614-7>
21. Jung J, Park O (2009) Synthetic approaches and biological activities of 4-hydroxycoumarin derivatives. *Molecules* 14(11):4790–4803. <https://doi.org/10.3390/molecules14114790>
22. Hamdi N, Puerta MC, Valera P (2008) Synthesis, structure, antimicrobial and antioxidant investigations of dicoumarol and related compounds. *Eur J Med Chem* 43(11):2541–2548. <https://doi.org/10.1016/j.ejmech.2008.03.038>
23. Choudhary MI, Fatima N, Khan KM et al (2006) New biscoumarin derivatives-cytotoxicity and enzyme inhibitory activities. *Med Chem* 14(23):8066–8072. <https://doi.org/10.1016/j.bmc.2006.07.037>
24. Reddy DS, Kongot M, Singh V et al (2021) Biscoumarin–pyrimidine conjugates as potent anticancer agents and binding mechanism of hit candidate with human serum albumin. *Arch Pharm (Weinheim)* 354(1):2000181–2000195. <https://doi.org/10.1002/ardp.202000181>
25. Manolov I, Maichle-Moessmer C, Nicolova I et al (2006) Synthesis and anticoagulant activities of substituted 2,4-diketochromans, biscoumarins, and chromanocoumarins. *Arch Pharm (Weinheim)* 339(6):319–326. <https://doi.org/10.1002/ardp.200500149>
26. Chaudhary G, Goyal S, Poonia P (2010) *Lawsonia inermis* linnaeus: a phytopharmacological review. *Int J Pharm Sci Drug Res* 2(2):91–98
27. De Oliveira AS, Brighente I, Lund R et al (2017) Antioxidant and antifungal activity of naphthoquinones dimeric derived from lawsone. *J Biosci Med* 5(2):39–48. <https://doi.org/10.4236/jbm.2017.52004>
28. De Araújo M, De Souza P, De Queiroz A et al (2014) Synthesis, leishmanicidal activity and theoretical evaluations of a series of substituted bis-2-hydroxy-1,4-naphthoquinones. *Molecules* 19(9):15180–15195. <https://doi.org/10.3390/molecules190915180>
29. Novais J, Rosandiski A, De Carvalho C et al (2020) Efficient synthesis and antibacterial profile of bis(2-hydroxynaphthalene-1,4-dione). *Curr Top Med Chem* 20(2):121–131. <https://doi.org/10.2174/1568026619666191210160342>
30. Sharma G, Kumar SV, Wahab HA (2018) Molecular docking, synthesis, and biological evaluation of naphthoquinone as potential novel scaffold for H5N1 neuraminidase inhibition. *J Biomol Struct Dyn* 36(1):233–242. <https://doi.org/10.1080/07391102.2016.1274271>
31. Mazumder A, Wang S, Neamati N et al (1996) Antiretroviral agents as inhibitors of both human immunodeficiency virus type 1 integrase and protease. *J Med Chem* 39(13):2472–2481. <https://doi.org/10.1021/jm960074e>
32. Khurana JM, Kumar S (2009) Tetrabutylammonium bromide (TBAB): a neutral and efficient catalyst for the synthesis of biscoumarin and 3,4-dihydropyrano[c]chromene derivatives in water and solvent-free conditions. *Tetrahedron Lett* 50(28):4125–4127. <https://doi.org/10.1016/j.tetlet.2009.04.125>
33. Mehrabi H, Abusaidi H (2010) Synthesis of biscoumarin and 3,4-dihydropyrano[c]chromene derivatives catalysed by sodium dodecyl sulfate (SDS) in neat water. *J Iran Chem Soc* 7(4):890–894. <https://doi.org/10.1007/BF03246084>
34. Tabatabaie K, Heidari H, Khorshidi A et al (2012) Synthesis of biscoumarin derivatives by the reaction of aldehydes and 4-hydroxycoumarin using ruthenium (III) chloride hydrate as a versatile homogeneous catalyst. *J Serbian Chem Soc* 77(4):407–413. <https://doi.org/10.2298/JSC110427189T>
35. Heravi MM, Sadjadi S, Haj NM et al (2009) Role of various heteropolyacids in the reaction of 4-hydroxycoumarin, aldehydes and ethylcyanoacetate. *Catal Commun* 10(13):1643–1646. <https://doi.org/10.1016/j.catcom.2009.04.031>
36. Khurana JM, Kumar S (2010) Ionic liquid: an efficient and recyclable medium for the synthesis of octahydroquinazolinone and biscoumarin derivatives. *Monatsh Chem Chem Mon* 141(5):561–564. <https://doi.org/10.1007/s00706-010-0306-4>
37. Thuy Giang LN, Tuyet Anh DT, Thi Phuong H et al (2021) DMAP-catalyzed efficient and convenient approach for the synthesis of 3,3'-(arylmethylene)bis(2-hydroxynaphthalene-1,4-dione)

- derivatives. *Nat Prod Commun* 16(9):1934578X2110458. <https://doi.org/10.1177/1934578X211045808>
38. Kaur G, Singh D, Singh A et al (2021) Camphor sulfonic acid catalyzed facile and general method for the synthesis of 3,3'-(arylmethylene)bis(4-hydroxy-2H-chromen-2-ones), 3,3'-(arylmethylene)bis(2-hydroxynaphthalene-1,4-diones) and 3,3'-(2-oxindoline-3,3'-diyl)bis(2-hydroxynaphthalene-1,4-dione) derivatives at room temperature. *Synth Commun* 51(7):1045–1057. <https://doi.org/10.1080/00397911.2020.1856877>
39. Mitra B, Ghosh P (2021) Humic acid: a biodegradable organo-catalyst for solvent-free synthesis of bis(indolyl)methanes, bis(pyrazolyl)methanes, bis-coumarins and bis-lawsone. *ChemistrySelect* 6(1):68–81. <https://doi.org/10.1002/slct.202004245>
40. Wang H, Wang Z, Wang C et al (2014) Lipase catalyzed synthesis of 3,3'-(arylmethylene)bis(2-hydroxynaphthalene-1,4-dione). *RSC Adv* 4(67):35686–35689. <https://doi.org/10.1039/C4RA06516F>
41. Tisseh ZN, Bazgir A (2009) An efficient, clean synthesis of 3,3'-(arylmethylene)bis(2-hydroxynaphthalene-1,4-dione) derivatives. *Dyes Pigm* 83(2):258–261. <https://doi.org/10.1016/j.dyepig.2008.09.003>
42. De Oliveira AS, Llanes LC, Nunes RJ et al (2014) Use of ultrasound and microwave irradiation for clean and efficient synthesis of 3,3'-(arylmethylene)bis(2-hydroxynaphthalene-1,4-dione) derivatives. *Green Sustain Chem* 4(4):177–184. <https://doi.org/10.4236/gsc.2014.44023>
43. Brahmachari G (2015) Sulfamic acid-catalyzed one-pot room temperature synthesis of biologically relevant bis-lawsone derivatives. *ACS Sustain Chem Eng* 3(9):2058–2066. <https://doi.org/10.1021/acssuschemeng.5b00325>
44. Asghari-Haji F, Rad-Moghadam K, Mahmoodi NO (2016) An efficient approach to bis-benzoquinonylmethanes on water under catalysis of the bio-derived O-carboxymethyl chitosan. *RSC Adv* 6(33):27388–27394. <https://doi.org/10.1039/C5RA26580K>
45. Shaikh S, Rasal S, Ramana MMV (2021) Ultrasound assisted synthesis of pyrano[3,2-b]pyran and 7-tosyl-4,7-dihydropyrano[2,3-e]indole scaffolds using barium titanate nanoparticles. *React Kinet Mech Catal* 133(1):405–424. <https://doi.org/10.1007/s11144-021-01972-3>
46. Shaikh S, Yellapurkar I, Ramana MMV (2021) Ultrasound assisted one-pot synthesis of novel antipyrine based α -aminophosphonates using TiO₂/carbon nanotubes nanocomposite as a heterogeneous catalyst. *React Kinet Mech Catal* 134(2):917–936. <https://doi.org/10.1007/s11144-021-02110-9>
47. Hummers WS, Offeman RE (1958) Preparation of graphitic oxide. *J Am Chem Soc* 80(6):1339–1339. <https://doi.org/10.1021/ja01539a017>
48. Li D, Müller MB, Gilje S et al (2008) Processable aqueous dispersions of graphene nanosheets. *Nat Nanotechnol* 3(2):101–105. <https://doi.org/10.1038/nnano.2007.451>
49. Men X, Wu Y, Chen H et al (2017) Facile fabrication of TiO₂/Graphene composite foams with enhanced photocatalytic properties. *J Alloys Compd* 703:251–257. <https://doi.org/10.1016/j.jallcom.2017.01.353>
50. Li Y, Zhang S, Li N et al (2020) A highly sensitive and selective molecularly imprinted electrochemical sensor modified with TiO₂-reduced graphene oxide nanocomposite for determination of podophyllotoxin in real samples. *J Electroanal Chem* 873:114439–114437. <https://doi.org/10.1016/j.jelechem.2020.114439>
51. Nipane SV, Lee S, Gokavi GS et al (2018) In situ one pot synthesis of nanoscale TiO₂-anchored reduced graphene oxide (RGO) for improved photodegradation of 5-fluorouracil drug. *J Mater Sci Mater Electron* 29(19):16553–16564. <https://doi.org/10.1007/s10854-018-9749-x>
52. John D, Rajalakshmi AS, Lopez RM et al (2020) TiO₂-reduced graphene oxide nanocomposites for the trace removal of diclofenac. *SN Appl Sci* 2(5):840–855. <https://doi.org/10.1007/s42452-020-2662-y>
53. Sher Shah MSA, Park AR, Zhang K et al (2012) Green synthesis of biphasic TiO₂-reduced graphene oxide nanocomposites with highly enhanced photocatalytic activity. *ACS Appl Mater Interfaces* 4(8):3893–3901. <https://doi.org/10.1021/am301287m>
54. Adamu H, Dubey P, Anderson JA (2016) Probing the role of thermally reduced graphene oxide in enhancing performance of TiO₂ in photocatalytic phenol removal from aqueous environments. *Chem Eng J* 284:380–388. <https://doi.org/10.1016/j.cej.2015.08.147>
55. Deshmukh SP, Kale DP, Kar S et al (2020) Ultrasound assisted preparation of rGO/TiO₂ nanocomposite for effective photocatalytic degradation of methylene blue under sunlight. *Nano-Struct Nano-Objects* 21:100407–100411. <https://doi.org/10.1016/j.nano.2019.100407>
56. Tan L, Ong W, Chai S et al (2013) Reduced graphene oxide-TiO₂ nanocomposite as a promising visible-light-active photocatalyst for the conversion of carbon dioxide. *Nanoscale Res Lett* 8(1):465–473. <https://doi.org/10.1186/1556-276X-8-465>
57. Benjwal P, Kumar M, Chamoli P et al (2015) Enhanced photocatalytic degradation of methylene blue and adsorption of arsenic (III) by reduced graphene oxide (rGO)-metal oxide (TiO₂/Fe₃O₄) based nanocomposites. *RSC Adv* 5(89):73249–73260. <https://doi.org/10.1039/C5RA13689J>
58. Kocijan M, Ćurković L, Radošević T et al (2020) Photocatalytic degradation of organic pollutant using TiO₂/rGO nanocomposites under simulated sunlight. *Nanomater Sci Eng* 2(4):162–169. <https://doi.org/10.34624/nmse.v2i4.21063>
59. Yu L, Wang L, Sun X et al (2018) Enhanced photocatalytic activity of rGO/TiO₂ for the decomposition of formaldehyde under visible light irradiation. *J Environ Sci* 73:138–146. <https://doi.org/10.1016/j.jes.2018.01.022>
60. Kocijan M, Ćurković L, Radošević T (2021) Enhanced photocatalytic activity of hybrid rGO@TiO₂/CN Nanocomposite for organic pollutant degradation under solar light irradiation. *Catalysts* 11(9):1023–1038. <https://doi.org/10.3390/catal11091023>
61. Zeydi MM, Mahmoodi N (2016) Nano TiO₂@KSF as a high-efficient catalyst for solvent-free synthesis of biscoumarin derivatives. *Int J Nano Dimens* 7(2):174–180
62. Shamsaddini A, Sheikhhosseini E (2014) Synthesis of 3,3-Arylidene Bis(4-Hydroxycoumarin) catalyzed by p-Doecylbenzenesulfonic acid (DBSA) in aqueous media and microwave irradiation. *Int J Org Chem* 4(2):135–141. <https://doi.org/10.4236/ijoc.2014.42015>
63. Shirini F, Lati MP (2017) BiVO₄-NPs: an efficient nanocatalyst for the synthesis of biscoumarins, bis(indolyl)methanes and 3,4-dihydropyrimidin-2(1H)-ones (thiones) derivatives. *J Iran Chem Soc* 14(1):75–87. <https://doi.org/10.1007/s13738-016-0959-y>
64. Babaei H, Montazeri N (2014) Nano TiO₂: an efficient catalyst for the synthesis of biscoumarins in aqueous medium. *Orient J Chem* 30(2):577–280. <https://doi.org/10.13005/ojoc/300223>
65. Khodabakhshi S, Marahel F, Rashidi A et al (2015) A green synthesis of substituted coumarins using nano graphene oxide as recyclable catalyst. *J Chin Chem Soc* 62(5):389–392. <https://doi.org/10.1002/jccs.201400349>
66. Riaz MT, Yaqub M, Shafiq Z et al (2021) Synthesis, biological activity and docking calculations of bis-naphthoquinone

derivatives from lawsone. *Bioorg Chem* 114:105069–105071.
<https://doi.org/10.1016/j.bioorg.2021.105069>

Publisher's Note Springer Nature remains neutral with regard to jurisdictional claims in published maps and institutional affiliations.

Springer Nature or its licensor (e.g. a society or other partner) holds exclusive rights to this article under a publishing agreement with the author(s) or other rightsholder(s); author self-archiving of the accepted manuscript version of this article is solely governed by the terms of such publishing agreement and applicable law.

Authors and Affiliations

Sarfaraz Shaikh^{1,2}  · Ishita Yellapurkar¹ · Sonal Bhabal¹ · M. M. V. Ramana¹ · Julekha A. Shaikh³

✉ Sarfaraz Shaikh
sarfarazshaikh@rizvicollege.edu.in

¹ Department of Chemistry, University of Mumbai, Santacruz (E), 400 098 Mumbai, India

² Department of Chemistry, Rizvi College of Arts, Science and Commerce, Bandra (West), Mumbai 400 050, India

³ Department of Chemistry, Maharashtra College of Arts, Science and Commerce, 246-A, J.B.B. Marg, 400 008 Mumbai, India